AIP | Applied Physics Letters

Mirror-embedded microchannel for three-dimensional measurement of particle position

Sungyoung Choi and Je-Kyun Park

Citation: Appl. Phys. Lett. **93**, 191909 (2008); doi: 10.1063/1.3027058
View online: http://dx.doi.org/10.1063/1.3027058
View Table of Contents: http://apl.aip.org/resource/1/APPLAB/v93/i19
Published by the American Institute of Physics.

Mirror-embedded microchannel for three-dimensional measurement of particle position

Sungyoung Choi and Je-Kyun Park[a)]
Department of Bio and Brain Engineering, KAIST, 335 Gwahangno, Yuseong-gu, Daejeon 305-701, Republic of Korea

(Received 1 September 2008; accepted 24 October 2008; published online 12 November 2008)

To enable easy implementation of three-dimensional (3D) characterization of flowing objects, we have developed a mirror-embedded microchannel to obtain 3D positional information from two different orthogonal-axis images. A silicon mirror reflects the side view of the channel and enables simultaneous imaging of the top and side views of the channel with a single lens. The measurement principle was verified by observing fluorescent streams simultaneously in both horizontal and vertical directions of a microchannel and measuring 3D positions of 6 and 10-μm sized beads without any optical modification of a microscope and additional optical equipment. © *2008 American Institute of Physics*. [DOI: 10.1063/1.3027058]

Advances in microfluidic technology are revolutionizing cellular biology by providing the ability to spatiotemporally handle cellular objects or molecular compounds on a micrometer scale. Dissolved molecules or suspended cells can be manipulated in three dimensions (3D) inside microchannels even with small cross-sectional area. Slant grooves or obstacles in a microchannel have been used for generation of dynamic concentration gradients that vary in space and time,[1–3] and self-sorting of cellular objects such as microbeads and blood cells by hydrophoretic principles.[4–6] Cell rolling and migration on patterned substrates with cell adhesion molecules were exploited for selective transport of cells.[7] Although these microfluidic devices show spatiotemporally varying characteristics, their performances are mostly evaluated in two-dimensions (2D) for a certain time period. Some static concentration gradients can be characterized in 3D by reconstructing layer-by-layer images obtained from confocal microscope. However, it is still a challenge to measure 3D particle positions and fluid streams inside microfluidic channels in real time.

Flow diagnostic methods such as 3D microparticle image velocimetry (PIV) can be a potential strategy to address the above needs.[8–11] PIV is an optical method used to estimate the kinematics of the local fluid. Typical PIV techniques require seed particles that have no influence on fluid characteristics. The velocity information of the fluid is calculated by processing the motion of the small particles. Since PIV techniques are typically based on spherical seed particles, it is difficult to measure 3D locations and orientations of nonspherical particles such as red blood cells and DNA molecules in a continuous flow. The PIV techniques do not also allow for imaging the gradient formation of molecular compounds simultaneously in the horizontal and vertical directions of microchannels. Stereoscopic PIV can resolve these problems by recording two simultaneous but distinct off-axis views of the same object.[12–14] However, stereoscopic methods require a relatively complex and expensive system with two sets of camera and optical equipments. Typical stereoscopic methods also require calibration algorithms to reconstruct 3D images from two different off-axis images that prevent easy implementation of 3D measurement of particle positions and fluid streams in microchannels.

In this letter, we describe a mirror-embedded microchannel for 3D measurement of particle positions. As shown in Fig. 1, the device consists of a silicon mirror and poly(dimethylsiloxane) (PDMS) microchannel made by aligning and bonding two PDMS layers. The mirror ideally at 45° (θ) reflects the side view of the channel and enables simultaneous imaging of the top and side views of the channel with a single lens. At the same time, the distance (d) between the mirror and channel is within the depth of field (DOF) that is determined by the distance from the nearest object plane to the farthest plane in focus. Therefore, we can obtain 3D locations of particles without calibration by directly observing the in-focus side and top views of the mirror-embedded channel. We can also capture images for fluorescent streams simultaneously in both horizontal and vertical directions of the microchannel using a standard inverted microscope without any optical modification and additional optical equipments.

All devices were fabricated using multistep photolithography techniques (see Ref. 15). Fluorescent polystyrene beads with a diameter of 6 and 10 μm (Molecular Probes, Eugene, OR) were used to demonstrate 3D measurement of

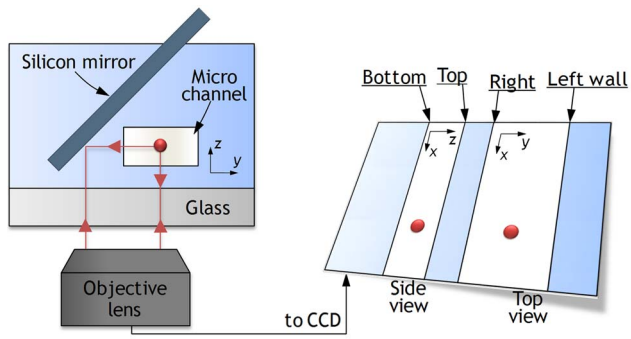

FIG. 1. (Color online) Mirror-embedded microchannel for simultaneously observing the in-focus side and top views of the channel. The mirror ideally at 45° reflects the side view of the channel and enables simultaneous imaging of the top and side views of the channel with a single lens. The distance between the mirror and channel is within the DOF that is determined by the distance from the nearest object plane to the farthest plane in focus.

[a)]Electronic mail: jekyun@kaist.ac.kr.

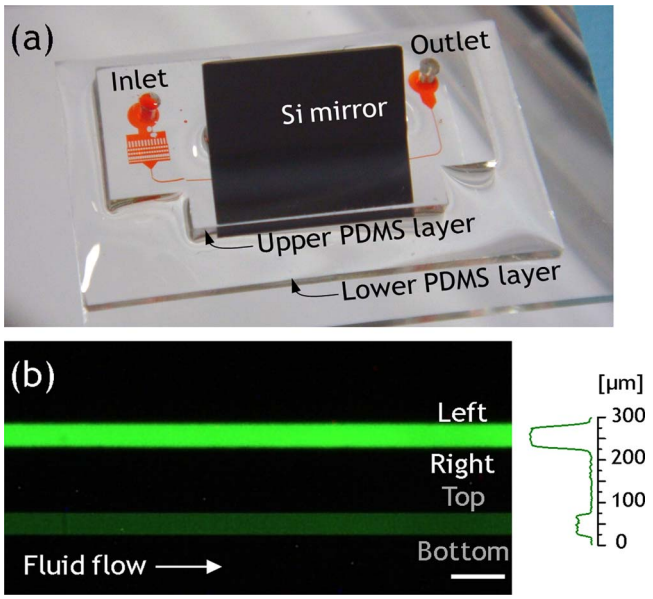

FIG. 2. (Color online) (a) Photograph of the mirror-embedded microchannel filled with a food dye. The silicon mirror (12 mm in width and 10 mm in length) is embedded in the PDMS device at an angle of 41°. The prefilter is used to remove dusts over 20 μm in diameter. (b) Fluorescence micrograph and intensity profile of the microchannel filled with FITC solution. The upper and lower stripes show the top and side views of the channel, respectively. The side view is an image reflected from the silicon mirror (scale bar=100 μm).

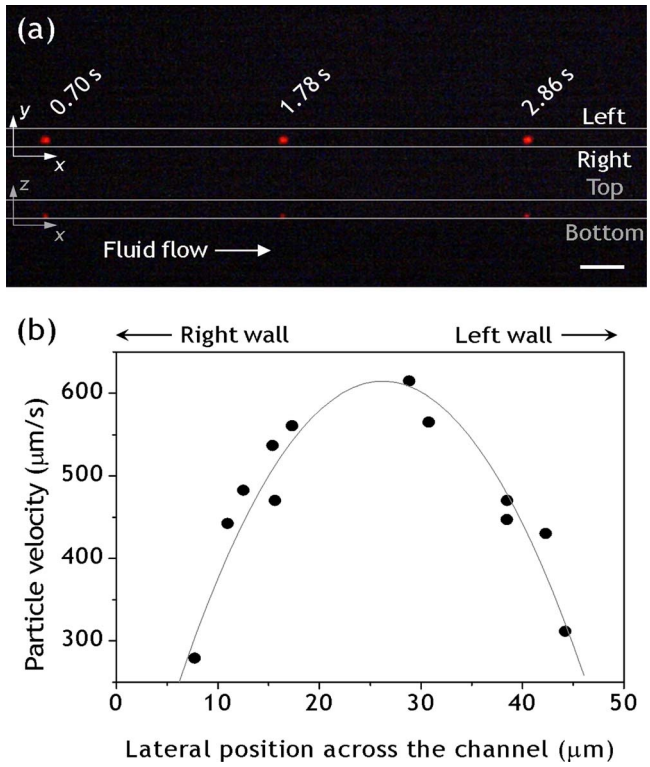

FIG. 3. (Color online) (a) Fluorescence micrograph showing a 10-μm-sized bead flowing the mirror-embedded microchannel. This figure was obtained by superimposing sequential particle images. The upper and lower images show the top and side views of the channel, respectively (scale bar =100 μm). (b) Velocity profile of 10-μm-sized beads flowing the channel in the xy-plane 5 μm apart above the bottom wall. The line is a polynomial fit of second order. The applied flow rate was 0.1 μl/min.

particle positions in the mirror-embedded microchannels. The beads were prepared in 2% pluoronic F68 solution (Sigma-Aldrich, St. Louis, MO). Fluorescein isothiocyanate (FITC) solution was prepared with a concentration of 20 μg/ml to visualize fluorescent streams simultaneously in both horizontal and vertical directions of the microchannel.

The microchannel was imaged through an inverted optical microscope (TS100, Nikon Co., Japan) and a Nikon Plan Apochromat objective lens with a magnification of 4× and a numerical aperture of 0.1. Microscopic images were taken with a charge coupled device (CCD) camera (DS-2MBWc, Nikon Co.). A syringe pump (Pump 11 Pico Plus, Harvard Apparatus, MA) was used to produce a continuous flow through the microchannel. A commercial image-analysis program, i-Solution (IMT i-Solution Inc., Korea) was used to measure the positions of particles inside the microchannel.

We demonstrated the proper functioning of the mirror-embedded microchannel by imaging the channel filled with FITC as shown in Fig. 2. The applied flow rate was 0.1 μl/min. The upper and lower stripes show the top and side views of the channel, respectively. The side-view width of 51.6 μm well corresponds to the mold thickness of 51.9 μm for the channel (50 μm in width). The fluorescence-intensity measurement shows that the average intensity of the top-view image is approximately four times higher than that of the side-view image reflected from the silicon mirror. This intensity attenuation of the reflected image is attributed to the low reflectance of a silicon wafer and a thin oxide layer on the wafer. The typical reflectance of silicon mirrors at wavelengths of 500–800 nm is approximately 35% that can make it difficult to image low light-level objects.[16] High-reflection (HR) coatings can be used to enhance reflection from silicon surfaces. Thin aluminum films as one of HR coatings were used to enhance a reflectance of silicon mirrors up to more than 80%.[16] This mirror-integrated device offers a simple means for flow diagnosis of fluorescent streams simultaneously in the horizontal and vertical directions of microchannels without any optical modification of microscopes.

The mirror-embedded channel can also be used to measure 3D positions of microparticles flowing microchannels. Figure 3(a) shows a sequential image of a moving 10-μm-sized particle in the linear channel. The particle was moving along the x-axis at the position (y,z) $=(17.3\ \mu\text{m}, 5.0\ \mu\text{m})$. Particle velocities were determined by dividing the moving distance over each time interval. As shown in Fig. 3(b), a parabolic velocity profile is formed across the channel width on the xy-plane 5 μm apart above the bottom wall. The particle velocity was 560.9 μm/s at the position $(y,z)=(17.3\ \mu\text{m}, 5.0\ \mu\text{m})$. The velocity was increased going toward the channel center: 1818.2 μm/s at $(y,z)=(25.0\ \mu\text{m}, 20.3\ \mu\text{m})$. Figure 4 shows the trajectory of a flowing 6-μm-sized bead in the grooved microchannel, imaged by fluorescence microscopy with a long-time exposure. As mentioned before, the lower intensity of the side view results from the low reflectance of the silicon mirror. The slanted groove patterns on the channel generate rotational flows by using a steady axial pressure gradient.[2,3] Such convective vortices make the bead move along the z-axis as well as the y-axis. As shown in Fig. 4, the 6-μm-sized bead travels back and forth between the right and left sidewalls. Before crossing from the right to the left wall, the bead begins to approach near the groove surfaces. At the crossing,

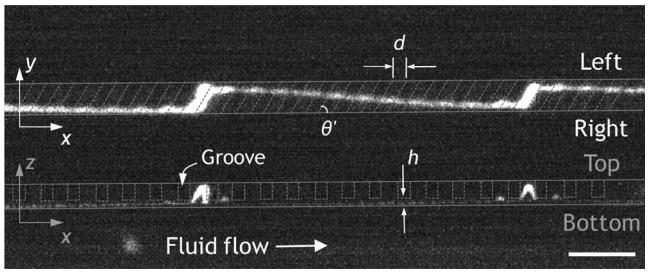

FIG. 4. Fluorescence stream of a 6-μm-sized bead flowing the microchannel (50 μm in width and 43 μm in height) with slanted grooves of $d=24$ μm, $\theta'=60°$, and $h=17$ μm. The upper and lower images show the top and side views of the channel, respectively (scale bar=100 μm).

the bead abruptly goes up to the top wall and moves down to the groove surfaces. The presented device will be helpful to understand 3D flow characteristics in the field of microfluidics.

When obtaining two images with different light-path lengths with a single objective lens, the DOF of the lens determines whether the images are in focus or out of focus. DOF is given by Inoué and Spring[17] as follows:

$$\mathrm{DOF} = \frac{n\lambda}{\mathrm{NA}^2} + \frac{ne}{\mathrm{NA}M}, \tag{1}$$

where n is the refractive index of the medium, λ is the wavelength of illuminating light, NA is the numerical aperture of the objective lens, M is the magnification of the system, and e is the pixel spacing of a CCD sensor. The calculated DOF from Eq. (1) is 115 μm for $\lambda=700$ nm and $e=24$ μm. This value is slightly smaller than the mirror-to-channel distance (d) of $\sim$150 μm. The insufficient DOF resulted in the blurring of the top-view image in Fig. 3(a). The 10-μm-sized bead was imaged larger than its real size. However, the particle positions (specifically, particle centers) were not affected by the blurring. A possible strategy to resolve this blurring problem is to introduce an objective lens with lower NA and higher DOF covering the mirror-to-channel distance. Also, it can be another solution for the blurring problem to put the silicon mirror closer to the channel.

In conclusion, we demonstrated a proof-of-principle mirror-embedded channel that allows 3D measurement of particle positions. The channel made of a single cast of PDMS ensures easy implementation of 3D measurement without any optical modification of a microscope and additional optical equipments. In practice, the current implementation may prove to be useful in the measurement of the positions and velocities of moving microparticles in the channel. However, pattering the channel with cell adhesion molecules will enable the extension of the application to cellular studies such as cell rolling and migration. This method can also be used for flow diagnosis of 2D hydrodynamic focusing devices and diffusion kinetics studies in microchannels by imaging fluorescent streams simultaneously in both horizontal and vertical directions of microchannels.

This work was supported by the Korea Science and Engineering Foundation (KOSEF) NRL Program grant funded by the Korean government (MEST) (Grant No. R0A-2008-000-20109-0) and by the Nano/Bio Science and Technology Program (Grant No. 2005-01291) of the MEST, Korea. The authors also thank the Chung Moon Soul Center for BioInformation and BioElectronics, KAIST.

[1] C.-H. Hsu and A. Folch, Appl. Phys. Lett. **89**, 144102 (2006).
[2] A. D. Stroock, S. K. W. Dertinger, A. Ajdari, I. Mezić, H. A. Stone, and G. M. Whitesides, Science **295**, 647 (2002).
[3] A. D. Stroock, S. K. Dertinger, G. M. Whitesides, and A. Ajdari, Anal. Chem. **74**, 5306 (2002).
[4] S. Choi and J.-K. Park, Lab Chip **7**, 890 (2007).
[5] S. Choi, S. Song, C. Choi, and J.-K. Park, Small **4**, 634 (2008).
[6] S. Choi and J.-K. Park, Anal. Chem. **80**, 3035 (2008).
[7] R. Karnik, S. Hong, H. Zhang, Y. Mei, D. G. Anderson, J. M. Karp, and R. Langer, Nano Lett. **8**, 1153 (2008).
[8] S. Y. Yoon and K. C. Kim, Meas. Sci. Technol. **17**, 2897 (2006).
[9] C. D. Meinhart, S. T. Wereley, and J. G. Santiago, Exp. Fluids **27**, 414 (1999).
[10] I. Grant, Proc. Inst. Mech. Eng., Part C: J. Mech. Eng. Sci. **211**, 55 (1997).
[11] S.-I. Satake, T. Kunugi, K. Sato, T. Ito, H. Kanamori, and J. Taniguchi, Meas. Sci. Technol. **17**, 1647 (2006).
[12] M. R. Bown, J. M. MacInnes, R. W. K. Allen, and W. B. J. Zimmerman, Meas. Sci. Technol. **17**, 2175 (2006).
[13] N. J. Lawson and J. Wu, Meas. Sci. Technol. **8**, 894 (1997).
[14] A. K. Prasad, Exp. Fluids **29**, 103 (2000).
[15] See EPAPS Document No. E-APPLAB-93-036846 for microfabrication methods including FIG. S1. For more information on EPAPS, see http://www.aip.org/pubservs/epaps.html.
[16] T. Babeva, S. Kitova, B. Mednikarov, and I. Konstantinov, Appl. Opt. **41**, 3840 (2002).
[17] S. Inoué and K. Spring, *Video Microscopy: The Fundamentals* (Plenum, New York, 1997).